Fusion Engineering and Design 162 (2021) 112099

Contents lists available at ScienceDirect

Fusion Engineering and Design

journal homepage: www.elsevier.com/locate/fusengdes

Joining tungsten with steel for DEMO: Simultaneous brazing by Cu-Ti amorphous foils and heat treatment

Diana Bachurina [a,*], Alexey Suchkov [a], Julia Gurova [a], Maxim Savelyev [a], Pavel Dzhumaev [a], Ilya Kozlov [a], Roman Svetogorov [b], Maria Leont'eva-Smirnova [a,c], Oleg Sevryukov [a]

[a] Department of Materials Science, National Research Nuclear University MEPhI, Moscow, 115409, Russia
[b] National Research Center «Kurchatov Institute», Moscow, 123182, Russia
[c] Bochvar High-Technology Research Institute of Inorganic Materials, Moscow 123098, Russia

ARTICLE INFO

Keywords:
DEMO
Ferritic-martensitic steel
Tungsten
First wall
Brazing

ABSTRACT

Development of a reliable technology to join tungsten with steel is essential for DEMO application; however, it is difficult due to large differences in their physical properties. To solve this problem, high-temperature brazing was carried out. Cu-Ti brazing alloys, which were rapidly solidified into foil, were used together with a compensating vanadium interlayer, so the EK-181 steel/Cu-28Ti/V/Cu-50Ti/W and EK-181/Cu-50Ti/V/Cu-50Ti/W brazed joints were obtained. The microstructures of the seams were investigated by optical microscopy, SEM (EDX, EBSD) and synchrotron XRD. Thermocycling and shear strength tests showed that Cu-28Ti wt. % brazing alloy ensures a firmer joint compared to Cu-50Ti wt. %. The Cu-28Ti wt. % brazing alloy was used to perform high-temperature brazing in the brazing mode equivalent to traditional EK-181 steel heat treatment. It showed that every step of the heat treatment affected the microstructures and the shear strength.

1. Introduction

The DEMO reactor (DEMOstration Power Station) is the next step after ITER (International Thermonuclear Experimental Reactor) on the way to a thermonuclear power plant. There are several designs for plasma-facing components that require firm joints between tungsten and steel [1–3]. However, it is hard to achieve a direct joint between tungsten and steel because of the differences between their physical properties, which cause high stresses. Several techniques to solve this problem were offered, such as liquid state, i.e. high-temperature brazing with brazing alloys or electroplated layers [4–6] and solid-state, like hot isostatic pressing, spark plasma sintering, etc. [7–11]. Both technique categories can be used with a compensating interlayer to decrease thermal stresses occurring in tungsten due to thermal loads.

The most convenient way to make a joint for complicated components is high-temperature brazing with thin elastic foils, which is used now for manufacturing ITER components [12–14]. This technology is widely used in aerospace [15] and nuclear [16,17] applications. Using amorphous filler alloys improves the quality of the joints due to high capillarity activity and a homogeneous composition in the whole filler, which results in a more homogeneous microstructure compared to powder fillers [18]. Brazing technology also allows making a simultaneous manufacturing process with thermal heat treatment (HT) of the materials to be joined (base materials). This fact is of big interest because most works present the results of joining technologies with a too high temperature in the manufacturing process for ferritic-martensitic steel. It is known that the mechanical properties of such steels decrease significantly after heating above 500 °C [19,20]. However, we can carry out brazing simultaneous with steel heat treatment, which means that no deterioration will occur during the manufacturing process. Due to this fact, we aimed to conduct simultaneous joining and heat treatment to investigate the influence of HT on the strength and microstructure. Moreover, it is important to investigate the microstructures of the brazed seams to assess the influence of the technology, interlayers' and filler alloys' composition to predict further technology improvements.

Accordingly, this work presents the results of joining tungsten with reduced activation ferritic martensitic (RAFM) steel RUSFER EK-181 by high-temperature brazing using rapidly solidified foil-type filler based on copper-titanium (Cu-Ti) alloys. A vanadium (V) interlayer was used to relieve the stresses in the base materials. A similar joining method was previously investigated as well [21]. The joining using

* Corresponding author.
E-mail address: dmbachurina@mephi.ru (D. Bachurina).

https://doi.org/10.1016/j.fusengdes.2020.112099
Received 28 July 2020; Received in revised form 9 October 2020; Accepted 29 October 2020
Available online 10 November 2020
0920-3796/

copper-germanium (Cu-Ge) brazing alloys, however, cannot achieve the required strength. Hence, Cu-Ti brazing alloys were used in this work to achieve higher strength. This work also aimed at investigating the influence of the brazing mode equivalent to traditional heat treatment (THT) of EK-181 steel on the microstructure and mechanical properties. Additionally, the phase-state investigated by Electron Backscatter Diffraction Analysis (EBSD). Structural analysis of brazed seam by X-ray diffraction (XRD) was first time carried out at the Kurchatov Synchrotron Radiation Source.

2. Materials and methods

2.1. Materials

The base materials used in this work were a ferritic-martensitic (FM) steel, RUSFER EK-181 (Fe–12Cr–2W–V–Ta–B, wt. %), in the initial (ferritic) state and commercially available tungsten (W) 99.96 % (RF Specification TU 48-19-57-91). Pure V 99.6 % was used as the interlayer.

Cu-Ti brazing alloys Cu-50Ti wt. % (STEMET™ 1203) and Cu-28Ti wt. % (STEMET™ 1204) were used in an amorphous state. The brazing alloys were solidified rapidly into 50 μm thick foils using spinning technology. STEMET™ brazing alloys are also used for fission reactor components [16]. As Cu cannot solute in W, a higher concentration of Ti is preferable to increase interaction of a brazing alloy with W. As for EK-181/V joint, both of the brazing alloys were used.

Two types of brazed joints were made:

- EK-181/Cu-28Ti/V/Cu-50Ti/W;
- EK-181/Cu-50Ti/V/Cu-50Ti/W.

Schemes of the specimens to be investigated are presented on Fig. 1. For the microstructure investigations, the materials were of the cylindrical form with diameter × height: EK-181 – 13 × 6 mm, W – 10 × 1 mm and square V – 13 × 0.5 mm and for the shear strength tests width × height × length: EK-181 – 7 × 7 × 20 mm, W – 7 × 1 × 7 mm and V – 7 × 0.5 × 7 mm. More details about the shear strength tests are presented elsewhere [21].

2.2. Methods

Brazing was carried out in a vacuum furnace ($p < 10^{-5}$ mmHg). The process was carried out with a fixed 100 g load. The initial gap between the base materials corresponded to the thickness of the brazing foil. Usually, brazing is carried out at a temperature of 20–40 °C higher than the melting point (T_m) of the filler alloy. However, in this work, brazing temperature T_b = 1100 °C was chosen, because it is used in a heat treatment process for the RUSFER EK-181 steel. This means that we can simultaneously carry out brazing and heat treatment of the steel.

In the first step (Section 3.1), a comparison of Cu-28Ti (T_m = 870 °C) and Cu-50Ti (T_m = 960 °C) was made at using mode № 1:

№1) 1100 °C with a 20 min dwell. This mode was chosen to compare the results with those represented in the previous work [21], where Cu-Ge brazing alloys were used. This section shows that using Cu-28Ti is preferable.

Mode № 2 was applied in the second step (Section 3.2):

№2) 1100 °C with a 60 min dwell +720 °C with a 180 min dwell corresponding to traditional heat treatment of EK-181 [22]. A graph of the modes is presented on Fig. 2. Only EK-181/Cu-28Ti/V/Cu-50Ti/W was investigated according to the results described in Section 3.1. An influence of 60 min dwell on the microstructure of the V/Cu-50Ti/W seam is presented in the Section 3.2.1, on the microstructure of the EK-181/Cu-28Ti/V seam – in the Section 3.2.2.

For the thermocycling test, the specimens were placed into a quartz

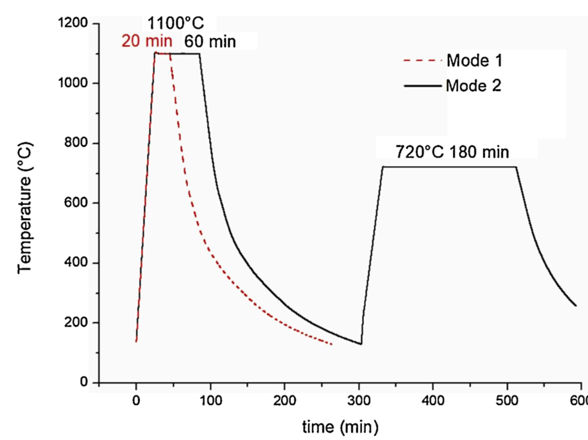

Fig. 2. Brazing modes.

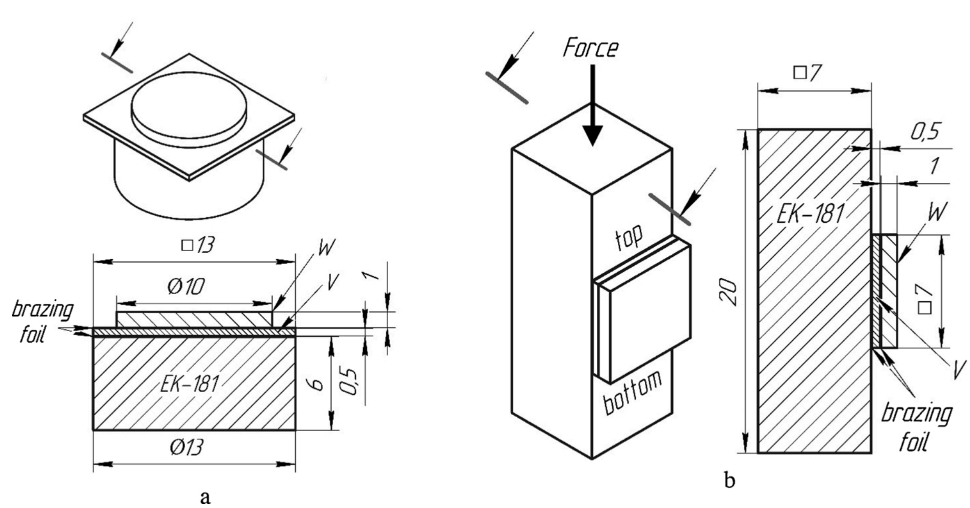

Fig. 1. Schemes of the specimens.
a) for the microstructure investigations before and after thermocycling.
b) for the shear strength tests before and after thermocycling.

ampoule with a vacuum faucet. The ampoule was vacuum evacuated to $p = 10^{-2}$ mmHg and the faucet was closed. Every 10 cycles, the ampoule was re-vacuumed to eliminate possible vacuum reduction due to air leakage. The ampoule with the specimens was heated in a tube furnace followed by quenching in water. No oxidation occurred during the test. The ampoules with specimens were heated to 700 °C (according to the exploitation temperature of the joint in the thimble of the HEMJ divertor [23]) and held for 10 min. 30 and 50 cycles of heating and quenching were conducted. This mode is tougher than the First Wall conditions, however, we used this mode to compare the results with those obtained by Cu-Ge brazing alloys. In addition, this cyclic mode provides express degradation of a joint and can be used as a methodology to conduct a fast comparison of filler alloy compositions or brazing modes.

Shear strength values (σ_τ) were obtained before thermocycling and after 50 cycles using an Instron 5569 materials testing machine (cross-head speed of 1 mm/min); three samples were measured for mode N°1 and five samples for mode N°2. The scheme of the tests was presented previously [21]. Microhardness $HV_{0,1}$ (100 g, 15 s dwell) was measured using FM-800 (Future-Tech) equipment.

The microstructures were studied using an MTI MM500 T optical microscope (OM). The samples were prepared metallographically following the standard technique and etched with 20 % HNO_3 + 20 % HF + 60 % glycerol solution for 30 s. Chemical compositions were measured with a JEOL JSM-6610LV scanning electron microscope using energy dispersive X-ray analysis (EDX). The phase-state was investigated using EBSD and synchrotron XRD. SEM images were obtained by backscattered electrons (BSE) and secondary electrons (SE).

EBSD analysis was carried out in a Zeiss EVO 50 XVP with Oxford Instruments Nordlys S detector and HKL CHANNEL5 program. The EBSD system works simultaneously with EDX, which allows receiving accurate results.

An X-ray diffraction study of the samples was performed using an X-ray structural analysis beamline from a Kurchatov Synchrotron Radiation Source [24]. Monochromatic irradiation with a 0.793569 Å (photon energy 15,623 eV) wavelength was used. A 150 μm thick sample was cut out from metallography specimen by wire machining. Positions of synchrotron ray (SR) beam were marked by red crosses. The specimen was placed in a magnetic holder perpendicular to the axis of the SR beam; the scheme is shown on Fig. 3. Diffraction patterns were collected by the 2D Rayonix SX165 detector, which was located at a distance of 80 mm, Debye-Scherrer (transmission) geometry was used with a 400 μm beam size. The exposure time was 1–6 min. To calibrate the sample-detector distance, we used a polycrystalline standard with a known position of the diffraction peaks; in this series of measurements, LaB_6 (NIST SRM 660a) powder was used. The two-dimensional diffraction patterns obtained by the detector were further integrated into the standard form of the dependence of the intensity on the scattering angle I (2θ), using Dionis software [25].

3. Results and discussions

3.1. Comparison of brazed joints EK-181/Cu-28Ti/V/Cu-50Ti/W and EK-181/Cu-50Ti/V/Cu-50Ti/W obtained using mode N° 1

To compare the results with previous work (brazing alloys of the Cu-Ge system [21]), the analysis of brazed joints was carried out in mode N°1. The analysis of the brazed V/Cu-50Ti/W seam obtained using mode N° 1 is also presented in that article.

3.1.1. Comparison of EK-181/Cu-28Ti/V and EK-181/Cu-50Ti/V microstructures

Fig. 4a, b shows the optical microstructure images of brazed seams EK-181/Cu-28Ti/V and EK-181/Cu-50Ti/V, respectively. Fig. 4c, d shows the concentration profiles of chemical elements plotted on SEM images. The peaks for titanium and carbon coincide, which indicates the formation of titanium carbides. The peak for copper coincides with the dips for the remaining elements; therefore, there are regions of a solid solution based on copper. It is noted that there is a significant diffusion of chromium from steel to vanadium, which should positively affect the adhesive strength of the joint. Thus, the following zones can be marked in both seams, which are marked in Fig. 4a, b: 1) ferritic-martensitic zone; 2) ferrite zone; ferritic grains are 30 μm larger in EK-181/Cu-50Ti/V; 3) the region with the formation of titanium carbides. This zone can be divided into two areas, a - small carbide placer inside ferrite grains and b - dense carbide placer. When using Cu-50Ti brazing alloy, the carbide placer in zone 3b is denser. Then, Zone 4) is the vanadium erosion region, i.e. vanadium boundaries are melted by the brazing alloy melt. Then comes Zone 5) pure vanadium.

Zone 2 was formed due to decarbonisation of the martensitic solid solution. This phenomena is usually observed while carbides form [5,21,26]. A difference in Zone 3 is observed using backscattered electrons (Fig. 4c, d). For EK-181/Cu-28Ti/V, in Zone 3b, the σ-phase of iron with vanadium is formed; the morphology and composition (57 Fe – 28 V – 8 Cr – 3 Ti – Cu, at. %) is identical to the observed σ-phase in the previous work [21]. Additionally, in the EK-181/Cu-28Ti/V seam there are zones with copper precipitates inside ferrite grains, this structural feature is observed only near the fillet regions. In the EK-181/Cu-50Ti/V no σ-phase nor Cu-precipitates within ferritic grains formed.

Fig. 4a, b also presents microhardness profiles. The microhardness of the steel in the initial state was ~ 270 $HV_{0.1}$ and it grew to 400 $HV_{0.1}$ after brazing. Decreasing microhardness was observed in Zone 2 up to 200 $HV_{0.1}$. The microhardness reached its highest value in Zone 3b.

3.1.2. Mechanical tests

The joints obtained using brazing mode N°1 were tested by a shear strength test. The tests were carried out before and after thermocycling.

The results of mechanical tests for shear prior to thermocycling are

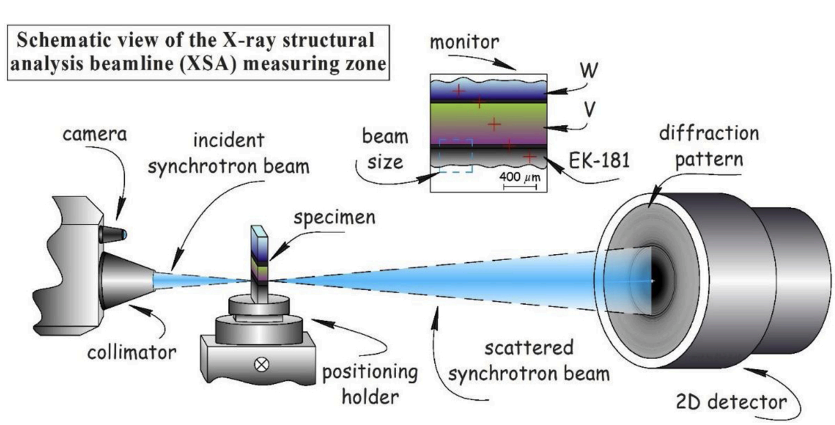

Fig. 3. Scheme of the XRD investigations of the specimens using a Kurchatov Synchrotron Radiation Source.

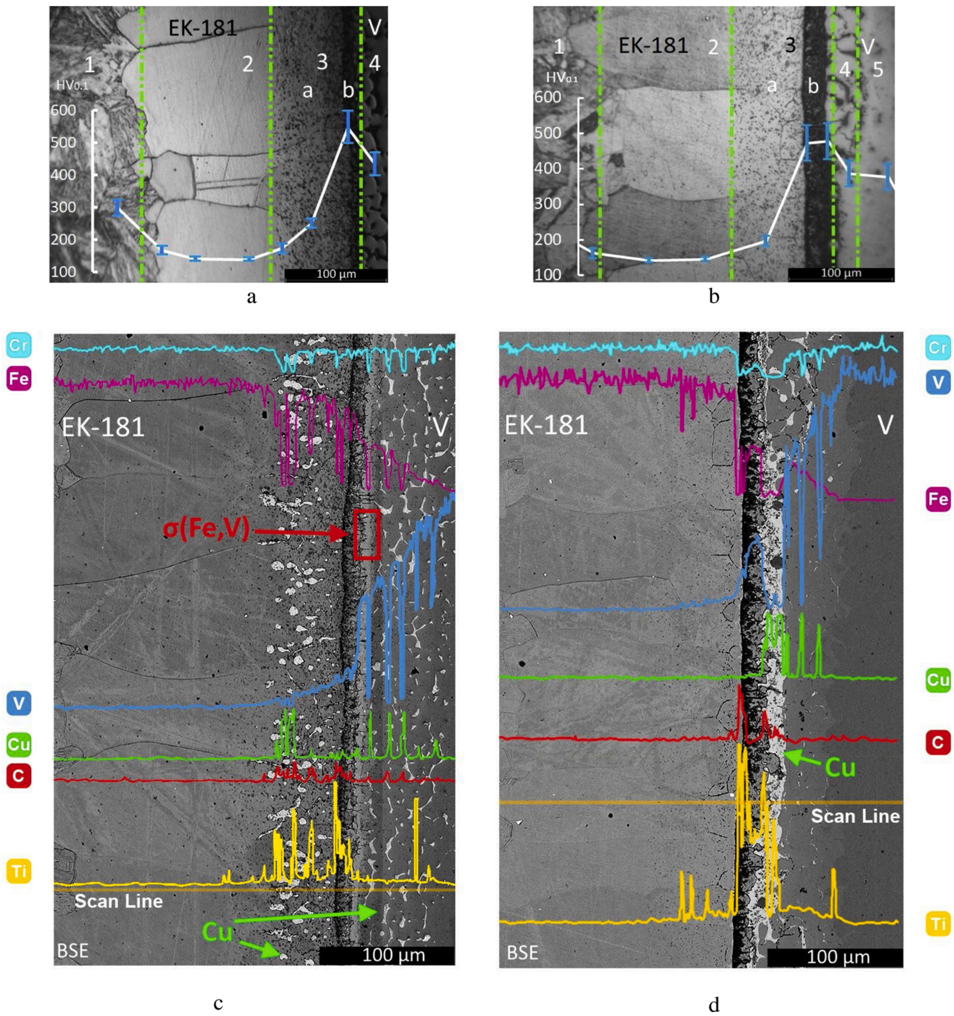

Fig. 4. Microstructure of EK-181/V brazed seams obtained using brazing mode № 1.
a) EK-181/Cu-28Ti/V OM with HV curve;
b) EK-181/Cu-50Ti/V OM with HV curve;
c) EK-181/Cu-28Ti/V BSE image with concentration profiles;
d) EK-181/Cu-50Ti/V BSE image with concentration profiles

205 ± 12 MPa for EK-181/Cu-28Ti/V/Cu-50Ti/W ("28Ti") and 98 ± 12 MPa for EK-181/Cu-50Ti/V/Cu-50Ti/W ("50Ti"). After 50 thermocycles, no microstructural changes occurred in the EK-181/V interface; however, crumblings from the V/W side appears in the structure of the brazed joints (Fig. 5). Such defects appear near (Fig. 5a) and within (Fig. 5b) fillet regions. Mechanical tests after 50 cycles give "28Ti" – 126 ± 40 MPa and "50Ti" – 30 ± 12 MPa. Failure occurred within W and V/W interface in both specimens, as shown in Fig. 6 where fractography and EDX spectra are presented. The colour of the rectangle in Fig. 6a corresponds to the EDX pattern in Fig. 6b. The vast majority of green № 1 pattern corresponds to pure W. The intensity of the red № 2 pattern identified that the failure occurred throughout the brazed seam V/W closer to V.

Due to the smaller amount of the carbide phase in the EK-181/V seam, as well as a higher value of shear strength, Cu-28Ti brazing alloy was chosen to study the effect of the traditional heat treatment of the steel on the quality of the brazed joint in Section 3.2.

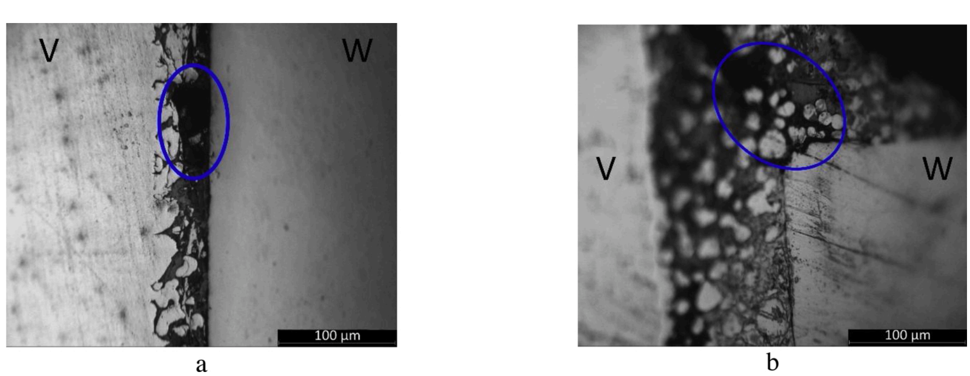

Fig. 5. Microstructure (OM) of the brazed seam V/Cu-50Ti/W obtained using brazing mode № 1 after thermocycling, blue ellipse outlines defects.
a) In the centre of the seam.
b) In the fillet region of the seam (For interpretation of the references to colour in this figure legend, the reader is referred to the web version of this article).

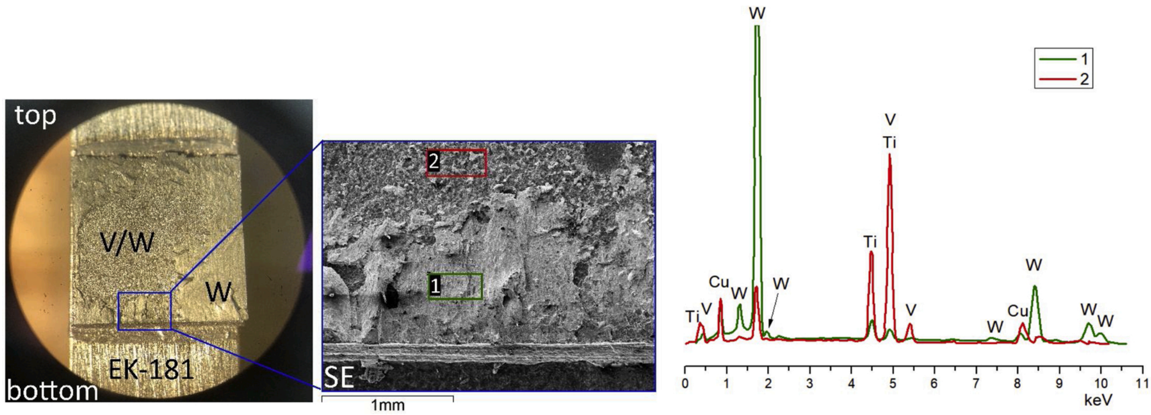

a b

Fig. 6. Fractography analysis of the brazed joint EK-181/Cu-50Ti/V/Cu-50Ti/W obtained using brazing mode N° 1 after thermocycling.
a) OM and SE images.
b) EDX spectra of encircled by green and red rectangles in a.

3.2. The study of brazed joint EK-181/Cu-28Ti/V/Cu-50Ti/W obtained using the brazing mode equal to the heat treatment of EK-181 (mode N° 2)

The dependence of the microstructure on the temperature-time mode and the changes in the mechanical properties were investigated to combine the processes of brazing and heat-treating the steel.

3.2.1. Brazed seam V/Cu-50Ti/W

As was mentioned earlier, microstructural analysis of brazed seam V/Cu-50Ti/W obtained using mode N°1 was carried out in the previous work [21]. Fig. 7 represents microstructures after 60 min dwell without ageing (Fig. 7a) and with ageing at 720 °C for 180 min, i.e. using mode N° 2 (Fig. 7b). With an increase in dwell time from 20 min to 60 min, residual filler alloy dissolves more due to longer interaction of the melt with the base materials. Additionally, rectangular phases formed, which was found to be TiC. The addition of ageing at 720 °C for 180 min does not affect the microstructure of this seam.

Thermocycling tests (Section 3.1.2) showed that the main destruction occurs in the V/W seam; hence, it is necessary to determine the reasons. Precise microstructural analyses were carried out by synchrotron XRD (Fig. 8) and EBSD.

To identify phases formed in the V/W seam, two different XRD patterns were obtained at slightly different positions (Fig. 8a, b). As synchrotron XRD gives low noise, even fine peaks can be analysed. To identify such tiny peaks magnified patterns of different areas of the main pattern are presented, e.g. rectangle 1 on the main pattern corresponds to a position of the magnified pattern 1 (Fig. 8a (1)) and etc. In Fig. 8a slightly bigger phases were identified: base V and W, TiC, CuTi and V_2C.

EDX analysis showed that no diffusion into W occurred. EDX analysis showed that V near residual filler alloy has the following composition, V – 10–20 Ti – 3–5 Cu at. %. EBSD analysis assessed this structure as a vanadium bcc crystalline structure. This means that this phase is a vanadium solid solution. The Cu amount in some points is two per cent more than the ultimate solubility of Cu in V at 1100 °C [27]; however, we believe that it can be caused by an error in the EDX analysis due to the presence of narrow streaks of a copper-containing phase.

CuTi peaks are clearly seen in Fig. 8a (2, 3). Other Cu-Ti phases were also observed, especially in SEM image: magnified BSE image of residual filler alloy zone is shown in Fig. 9a. There are two zones, N° 1—with an average composition of 54 Cu – 32 Ti – 14 V at. % and N° 2 with 72 Cu – 24 Ti – 4 V at. % (Fig. 9a). Since there is no triple Cu-Ti-V phase, this means that V replaces Ti in the Cu-Ti lattice. The former is believed to be CuTi as EBSD and XRD clearly identify it. The letter has a composition in the eutectic region in the Cu-Ti phase diagram [28], but no clear Kikuchi lines were obtained, however in Fig. 8b some peaks of the Cu_3Ti_2 and Cu_4Ti phases can be found. Hence, this region corresponds to fine eutectic (Cu_3Ti_2, Cu_4Ti).

As identified by synchrotron XRD, three types of carbides were formed, W_2C, V_2C, TiC. The TiC phase, which is shown in Fig. 7, has a wide homogeneity range and the average composition in the seam is 65 Ti– 30 C – 5 V + Cu at. %. Additionally, XRD identified V_2C (Fig. 8a) and W_2C (Fig. 7b), BSE image is shown on Fig. 9b. The phases were observed as a cluster and were found just close to the fillet; these phases were not found in the specimen obtained by 1100 °C/60 min without ageing.

Consequently, accumulation of two synchrotron XRD patterns with

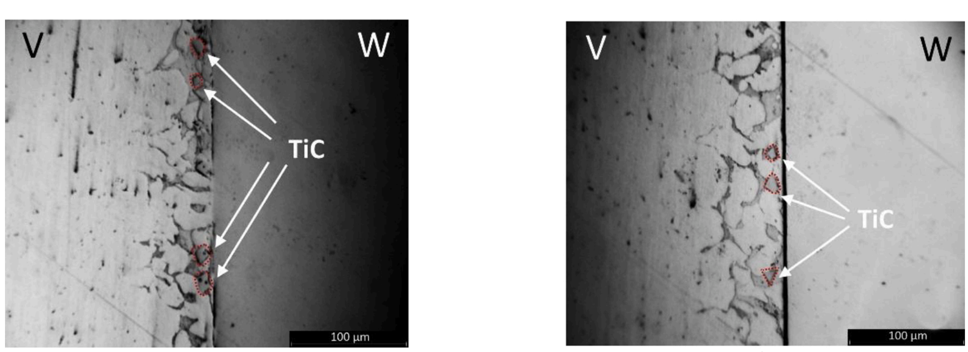

a b

Fig. 7. Microstructure (OM) of brazed seam V/Cu-50Ti/W obtained using brazing mode.
a) 1100 °C with 60 min dwell.
b) 1100 °C with 60 min dwell +720 °C with 180 min dwell (THT of EK-181).

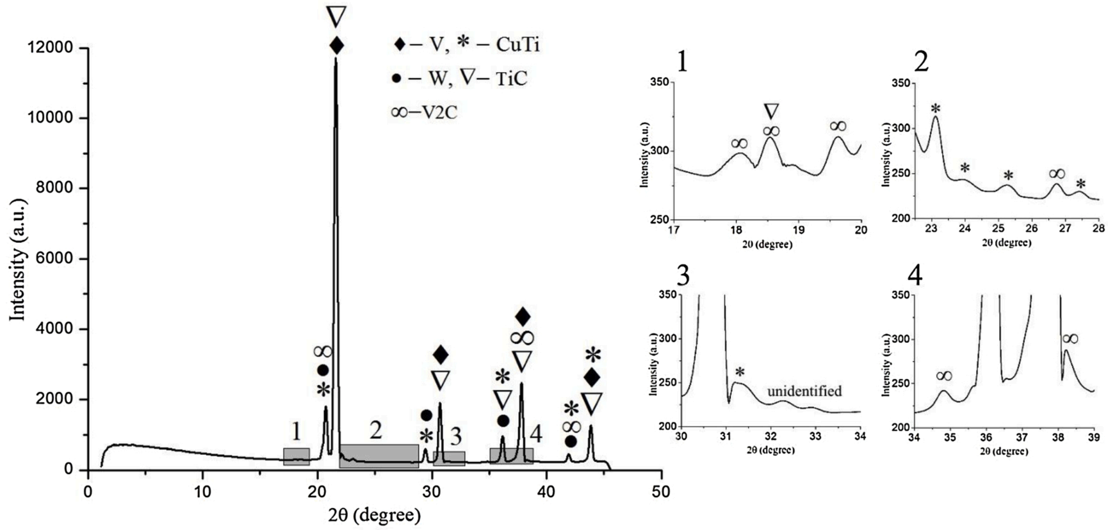

a

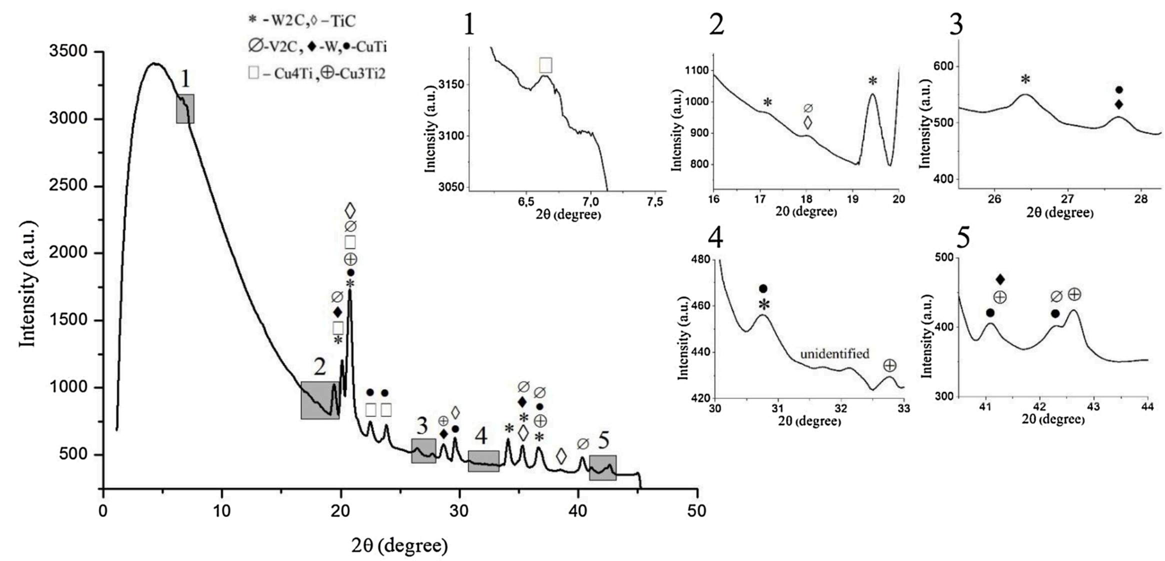

b

Fig. 8. Synchrotron XRD patterns obtained at the V/Cu-50Ti/W seam, brazing mode № 2.
a) synchrotron ray was positioned closer to V, 1–4 are the magnified images of the main pattern parts encircled by rectangles.
b) synchrotron ray was positioned closer to W, 1–5 are the magnified images of the main pattern parts encircled by rectangles.

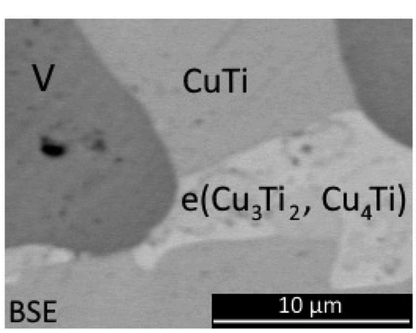

a

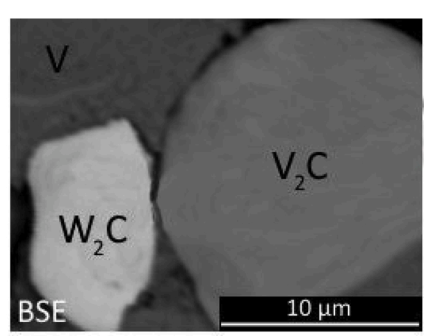

b

Fig. 9. Magnified BSE images of the V/Cu-50Ti/W seam, brazing mode № 2.
a) residual filler alloy zone.
b) W_2C, V_2C morphology.

EDX and EBSD analyses shows that the seam V/Cu-50Ti/W consists of the following phases: V, W, W_2C, V_2C, TiC, CuTi, Cu_3Ti_2, Cu_4Ti. However, some peaks between 31 and 34 degrees were not identified, which means that complex phases could have formed.

3.2.2. Brazed seam EK-181/Cu-28Ti/V

It was important to estimate whether the longer dwell time affected the grain growth of the ferritic phase. Fig. 10 represents microstructures after 60 min dwell without ageing (Fig. 10a) and with ageing at 720 °C for 180 min, i.e. using mode № 2 (Fig.10b). Compared to the brazed seam obtained using mode № 1 (Fig. 4a), ferritic grains grew to near 100 μm (zone 2 in Fig. 4). This is due to the increase in the exposure time at the brazing temperature, which leads to a more intense depletion of carbon from the steel. The microhardness of the steel after 1100 °C with 60 min dwell is ~400 $HV_{0.1}$, which is equal to the value in mode № 1. After mode № 2, the microhardness of the steel decreases to ~302 $HV_{0.1}$ (≈ 3 GPa), which corresponds to the value after THT [29].

To understand the influence of chemical elements on the microstructure of the joint at brazing mode, accurate investigations were carried out by EBSD, EDX and synchrotron XRD. XRD pattern is presented in Fig. 11. Similarly, to Fig. 8 (Section 3.2.1) to identify tiny peaks magnified patterns of different areas of the main pattern are presented, e.g. rectangle 1 on the main pattern corresponds to a position of the magnified pattern 1 (Fig. 11(1)) and etc.

XRD strongly correlates with EBSD and EDX. Zone 2 (Fig. 4a) is iron in the form of ferrite, Zone 3 (Fig. 4c) is σ(Fe, V), where legible Kikuchi lines were obtained.

As was mentioned in the Section 3.1.1, the distinctive feature of the compounds obtained using the Cu-Ti system is the presence of titanium carbides; however, vanadium carbides also formed, as is clear from XRD and EDX analysis. On the steel interface (to the left from σ(Fe, V)), only TiC formed with a composition similar to those that was found in Section 3.2.1: 65 Ti– 30 C – 5 V + Cu at. %. Morphology of the carbides is shown in Fig. 12a. TiC formed as fine precipitates within α-Fe and pure Cu.

On the V interface (to the right from σ(Fe, V)), both V-C and TiC formed. Vanadium carbides and TiC have different morphology. Vanadium carbides are elongated, while TiC has a rectangular form. Synchrotron XRD analysis identified two types of vanadium carbides: V_2C and V_6C_5, however we obtained legible Kikuchi lines only for V_2C. This can be related to the fine amount of V_6C_5. BSE images of carbides at V side are shown in Fig. 12b. Vanadium carbides formed close to Cu precipitates while TiC formed within vanadium carbides.

Cu_3Ti_2 phase was identified by synchrotron XRD, but we didn't find them both at steel and vanadium side. Obviously, this phase can be located within Cu precipitates.

According to synchrotron XRD, EBSD and EDX analysis, the seam consists of the following phases: V, α-Fe, Cu, TiC, σ(Fe, V), V_6C_5, V_2C, Cu_3Ti, but some peaks were not identified, which means that complex phases could have formed.

3.2.3. Mechanical tests of the EK-181/Cu-28Ti/V/Cu-50Ti/W joint

A shear strength test was carried out for the joint obtained by a brazing mode № 2 before and after thermocycling tests.

The shear strength of the EK-181/Cu-28Ti/V/Cu-50Ti/W brazed joint before thermocycling is 173 ± 25 MPa, which, within the error, coincides with the strength of the joint obtained by mode № 1. The shear strength after thermocycling is 50 ± 8 MPa, which is lower than the joint strength obtained by mode № 1. Fig. 13 presents fractography and EDX analysis of failed samples, the colour of a rectangle coincides with the colour of EDX pattern. Failure of the samples occurred in the V/W interface, especially in W, and in the EK-181/V interface both before and after thermocycling. In Fig. 13a, c yellow rectangles at the bottoms encircle V/W failure zone, pink rectangles above encircle failure at the EK-181/V interface. Analysis of the yellow zones shows that after the failure of pure tungsten (green № 1 pattern in Fig. 13b, c), a crack could propagated to the brazed seam enriched with vanadium (red № 2 pattern). Analysis of pink zones shows that failure occurred at the V/W seam (red № 2 pattern) and at the EK-181 side enriched with Ti (blue № 3 and № 4 patterns), which means that the failure of the V/EK-181 seam develops within titanium carbides. In Fig. 13c, on the steel surface (pink zone), two different contrasts are observed (blue № 3 and № 4), the difference is in the higher amount of Cu in area 3. After 50 thermocycles, the microstructure degrades similarly to that in mode № 1 (Section 3.1.2) — no changes at the EK-181/V interface (Fig. 14a) but crumblings appear from the V/W side both in the centre and fillet regions (Fig. 14b, c), which leads to the failure of the joint at this side during shear tests. It was found that V_2C and W_2C are responsible for weakening the joint at the mode № 2 as Cu-Ti phases fall out close to the carbides, as shown in SEM image of Fig. 14b. It is important to note that the microstructure was also investigated after 30 thermocycles and no degradation was observed.

4. Discussions

From comparison with the microstructure of brazed joints obtained using Cu-Ge brazing alloys [21], it can be noted that copper precipitates along the grain boundaries of ferrite in the EK-181/Cu-50Ti/V are completely absent and in the EK-181/Cu-28Ti/V are only observed in the seam when approaching the fillet region. Perhaps this may be because the formed carbide layer not only blocks the diffusion of iron to vanadium but also prevents the melting of steel grain boundaries because of its high melting point. Therefore, the brazing alloys' melt actively interacts with vanadium, which causes its erosion (zone 4). A smaller amount of erosion in the EK-181/Cu-50Ti/V seam is associated

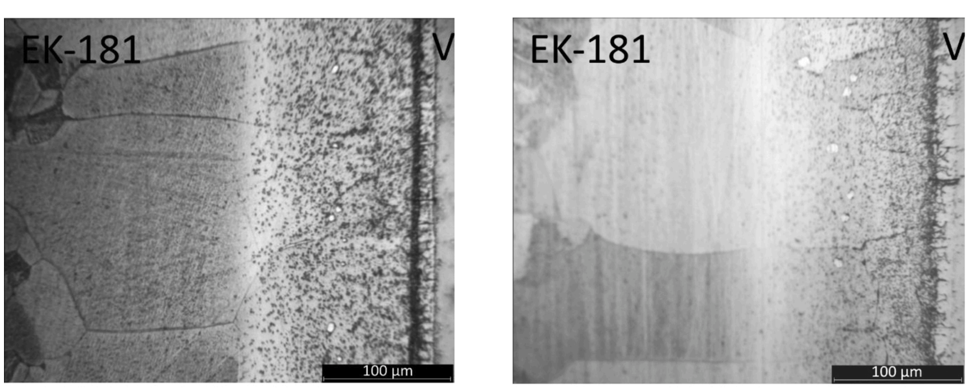

a b

Fig. 10. Microstructure (OM) of EK-181/ Cu-28Ti/V brazed seams obtained by brazing mode.
a) 1100 °C with 60 min dwell:
b) 1100 °C with 60 min dwell +720 °C with 180 min dwell (THT of EK-181).

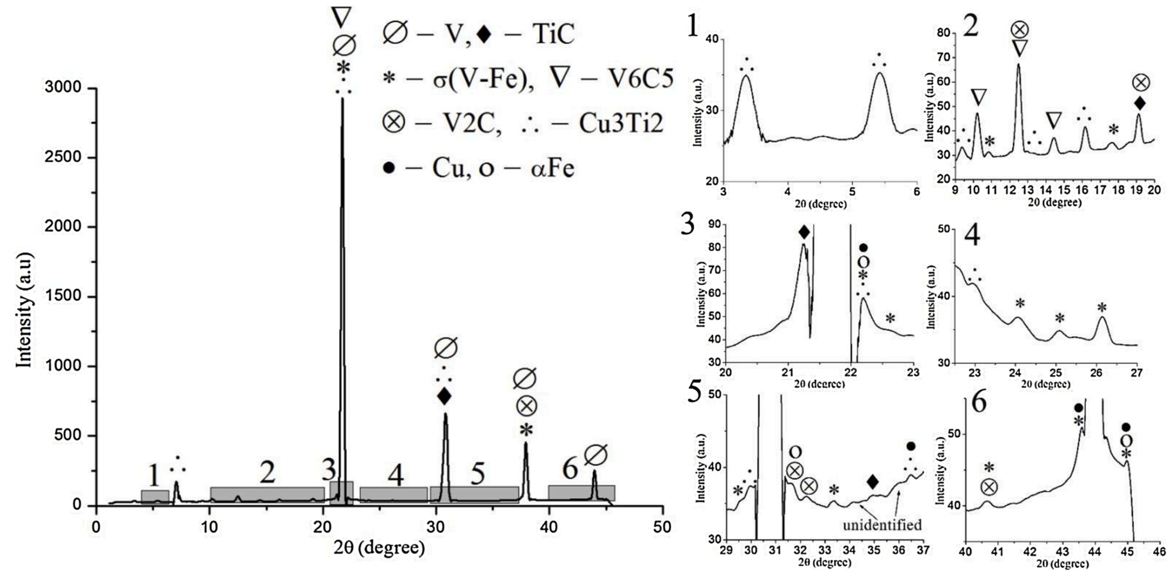

Fig. 11. Synchrotron XRD patterns obtained at EK-181/Cu-28Ti/V, brazing mode N° 2: 1-5 are the magnified images of the main pattern parts encircled by rectangles.

Fig. 12. Magnified BSE images of the EK-181/Cu-28Ti/V seam, brazing mode N° 2.
a) carbides morphology at the steel side (to the left from σ(Fe, V)).
b) carbides morphology at the vanadium side (to the right from σ(Fe, V)).

with a lower amount of Cu and the higher melting point of Cu-50Ti alloy. Moreover, in the EK-181/Cu-50Ti/V seam, the σ(Fe, V) phase was not observed, which may be due to a thicker carbide layer blocking the diffusion of iron from steel to vanadium. Nevertheless, a thick carbide layer decreases the ability to reduce thermally induced stressed by the presence of a compensating interlayer; this results in lower strength. Nevertheless, it is evident that the strength of the joints obtained by Cu-Ti brazing alloys is much higher than those obtained by Cu-Ge brazing alloys. The reason is a lower amount of Cu precipitates in the grain boundaries of the ferritic phase and an effect of crumbly carbides, which can work as strengthening precipitates.

Fig. 15 shows accumulated data from the shear strength tests. As was shown in Section 3.1.2 (Mode N° 1), the failure of the joints occurred in at the V/W interface, especially in W. Nevertheless, the shear strength of the EK-181/Cu-28Ti/V/Cu-50Ti/W is twofold higher than that of the EK-181/Cu-50Ti/V/Cu-50Ti/W, which proves that the microstructure of the EK-181/V seam significantly affects the reliability of the whole joint. For example, the more effective the EK-181/V seam relieves stresses, the fewer amount of crumblings in the V/W seam occurs after thermocycling. This means that structural phase state of a brazed EK-181/V seam plays an important role in decreasing thermal stresses. Therefore, it is evident that a smaller amount of carbides is beneficial; hence, the use of Cu-28Ti is preferred.

In all cases in Section 3.1.2 (Mode N° 1), failure of the joints occurred in W and V/W. Differently failure occurred in the joints discussed in Section 3.2.3 (Mode N° 2)— additionally to W and V/W interfaces failure occurred in the EK-181/V seam. We believe that this fact is related to the following. As the failure should have formed in the most stressed part – bottom region of a specimen, after failure had initiated in W, it then propagated through the weakest part of the joint. In the case of mode N° 1, it is V/W due to the thick layer of remaining Cu-Ti alloy. However, in a case of Mode N° 2, the V/W seam was strengthened by prior dissolution in the base materials and the formation of TiC; therefore, the failure occurred in the EK-181/V seam as well. After ageing at 720 °C, softening of the joint took place according to microhardness measurement, which is why the joint obtained using Mode N° 2 endured a lower load. Moreover, the reason for the propagation of a failure to the EK-181/V interface could be an accumulation of stresses around carbides, as was noticed close to borides in [30]. In addition, diffusion of carbon to the W side through the whole thickness (500 µm) of the vanadium interlayer with the formation of different carbides in the V/W seam weakens the joint. The last phenomenon exists only when the dwell time at 1100 °C increases to 60 min; hence, this time is enough for carbon to diffuse and form carbides. It is important to mention that only

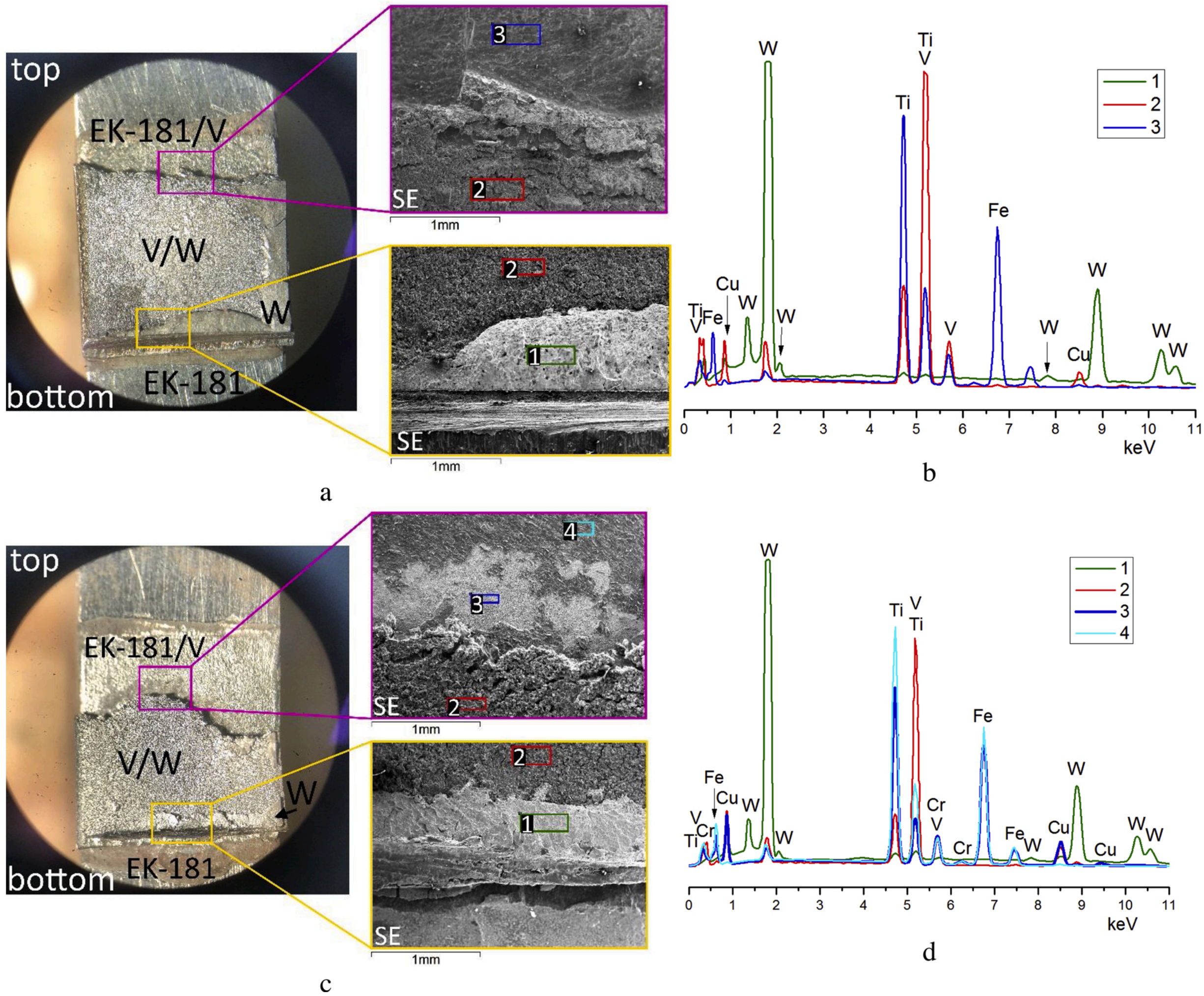

Fig. 13. Fractography analysis of brazed joint EK-181/Cu-28Ti/V/Cu-50Ti/W, brazing mode N°2 before thermocycling: a) OM and SE images b) EDX spectra of encircled by coloured rectangles in a after thermocycling: c) OM and SE images d) EDX spectra of encircled by coloured rectangles in c.

TiC carbides formed using the mode 1100 °C/60 min, while V_2C and W_2C formed in a case of 1100 °C/60 min + 720 °C/180 min as well as TiC. Hence the ageing was responsible for this fact. The size of these phases is big enough to decrease the strength and ability to decrease thermally induced stresses in tungsten.

Although the microstructure of the brazed seams is heterogeneous, sustainability against thermocycling tests is quite good as all the joints maintained integrity. For example in [31], cracks occurred after only 12 thermal cycles (720 °C – air quenching). Moreover, the results of shear tests are higher compared to other works [32,33].

Based on the results obtained while manufacturing ITER mock-ups [34], we can expect that upscaling will not reduce the quality of the joint. However further High Heat Flux experiments are needed to prove its applicability.

5. Conclusions

High-temperature brazing of an EK-181/W joint was carried out. A pure vanadium interlayer was used to compensate for thermal stresses. For the V/W seam, a rapidly solidified into foil Cu-50 Ti wt. % brazing alloy was used; for the EK-181/V seam Cu-28Ti wt. % and Cu-50Ti wt. % were used.

A comparison of brazed seams obtained using Cu-28Ti wt. % and Cu-50Ti wt. % was carried out using the mode of 1100 °C/20 min. The microstructure of the seams was analysed and thermocycling and mechanical tests were carried out. The strength of the joints before and after thermocycling tests are, respectively:

EK-181/Cu-28Ti/V/Cu-50Ti/W - 205 ± 12 MPa and 126 ± 40 MPa;

EK-181/Cu-50Ti/V/Cu-50Ti/W - 98 ± 12 MPa and 30 ± 12 MPa.

Based on these results, Cu-28Ti brazing alloy was selected for brazing the joint at a brazing mode equal to the traditional heat treatment (THT) of the EK-181 steel: 1100 °C/60 min with subsequent normalization and ageing at 720 °C. It was found that the longer the exposure time at 1100 °C is, the more the α-Fe grains grow. Additionally, increasing the exposure time leads to significant diffusion of carbon to the W interface through the whole vanadium interlayer. Ageing at 720 °C for 180 min enhances this effect. As a result, TiC forms at 1100 °C/60 min and TiC, V_2C, W_2C at 1100 °C/60 min +720 °C/180 min. The latter phases are responsible for the significant weakening of the joint after thermocycling.

The strength of the brazed EK-181/Cu-28Ti/V/Cu-50Ti/W joint obtained using the THT mode before thermocycling coincides with the mode of 1100 °C/20 min within the error and is equal to 173 ± 25 MPa. However, after thermocycling, shear strength drops to 50 ± 8 MPa.

Comparing the results with Cu-Ge brazing alloys, it is evident that the use of Cu-28Ti alloy is preferable. Further investigations under DEMO relevant conditions for EK-181/V/W joint should be carried out with the use of Cu-28Ti filler alloy, especially under the First Wall operating temperatures.

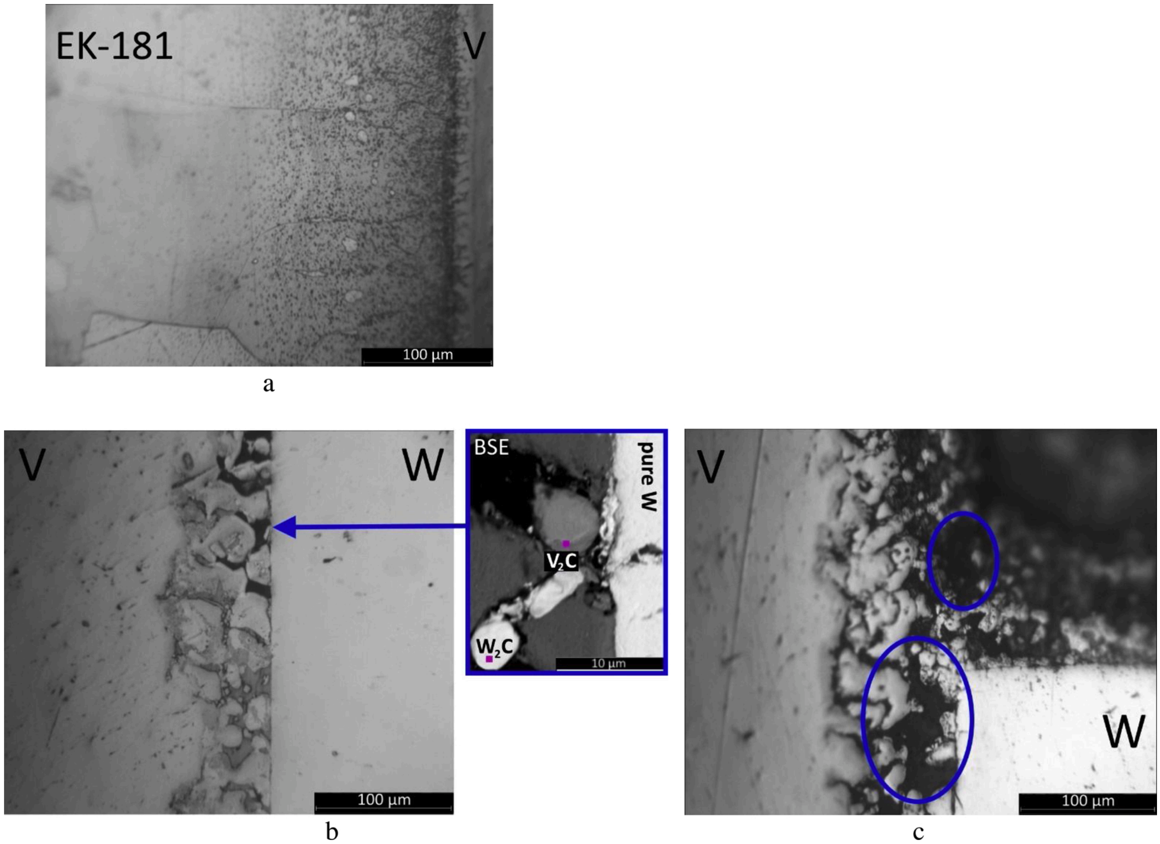

Fig. 14. Microstructures (OM) of the brazed joint EK-181/Cu-28Ti/V/Cu-50Ti/W obtained by brazing mode № 2 after thermocycling.
a) EK-181/ Cu-28Ti/V brazed seams.
b) Centre of the V/Cu-50Ti/W seam + BSE image showing degradation near W2C and V2C.
c) Fillet region of the V/Cu-50Ti/W seam, blue ellipses outline defects.

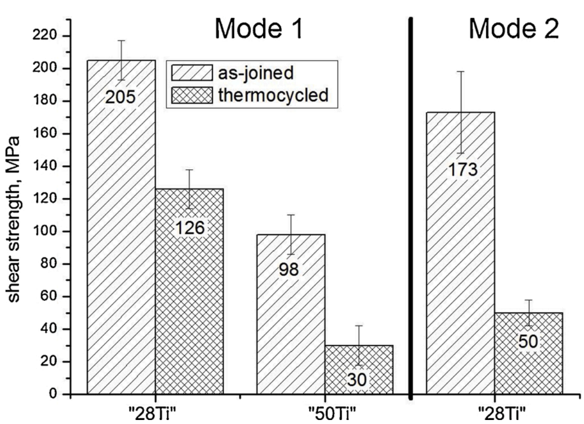

Fig. 15. Shear strength of the joints.
“28Ti” – EK-181/Cu-28Ti/V/Cu-50Ti/W.
“50Ti” - EK-181/Cu-50Ti/V/Cu-50Ti/W.

CRediT authorship contribution statement

Bachurina Diana: Investigation, Validation, Writing - original draft. **Suchkov Alexey:** Conceptualization, Methodology, Writing - review & editing. **Gurova Julia:** Visualization, Data curation. **Savelyev Maxim:** Investigation. **Dzhumaev Pavel:** Investigation. **Kozlov Ilya:** Formal analysis. **Svetogorov Roman:** Resources. **Maria Leont’eva-Smirnova:** Resources, Investigation. **Sevryukov Oleg:** Supervision.

Declaration of Competing Interest

The authors report no declarations of interest.

Acknowledgments

The work was funded by The Council for Grants of the President of the Russian Federation.

The investigation of the EK-181/V seam microstructure was funded by RFBR according to the research project № 18-32-00147.

Appendix A. Supplementary data

Supplementary material related to this article can be found, in the online version, at doi:https://doi.org/10.1016/j.fusengdes.2020.112099.

References

[1] T. Melichar, O. Frýbort, L. Vála, P. Zácha, I. Fernández, D. Rapisarda, Optimization of the first wall helium cooling system of the European DCLL using CFD approach, Fusion Eng. Des. 124 (2017) 426–431, https://doi.org/10.1016/j.fusengdes.2017.02.015.
[2] L.V. Boccaccini, G. Aiello, J. Aubert, C. Bachmann, T. Barrett, A. Del Nevo, D. Demange, L. Forest, F. Hernandez, P. Norajitra, G. Porempovic, D. Rapisarda, P. Sardain, M. Utili, L. Vala, Objectives and status of EUROfusion DEMO blanket studies, Fusion Eng. Des. 109–111 (2016) 1199–1206, https://doi.org/10.1016/j.fusengdes.2015.12.054.
[3] J. Aubert, G. Aiello, R. Boullon, F.A. Hernández, J.C. Jaboulay, DEMO breeding blanket helium cooled first wall design investigation to cope high heat loads, Fusion Eng. Des. (2019) 0–1, https://doi.org/10.1016/j.fusengdes.2019.01.009.

[4] Q. Cai, W. Liu, Y. Ma, Z. Wang, Diffusion brazing of tungsten and steel using Ti-Ni liquid phase forming interlayer, Fusion Eng. Des. 91 (2015) 67–72, https://doi.org/10.1016/j.fusengdes.2014.12.029.

[5] J. de Prado, M. Sánchez, A. Ureña, Development of brazing process for W–EUROFER joints using Cu-based fillers, Phys. Scr. T167 (2016) 014022, https://doi.org/10.1088/0031-8949/T167/1/014022.

[6] W. Zhu, J. Qiang, Y. Wang, J. Sun, J. Wang, Y. Lian, F. Feng, X. Liu, A Ti-Fe-Sn thin film assembly for joining tungsten and reduced activation ferritic-martensitic steels, Mater. Des. 125 (2017) 55–61, https://doi.org/10.1016/j.matdes.2017.03.060.

[7] C. Tan, C. Wang, S. Wang, G. Wang, L. Ji, Y. Tong, X.M. Duan, Investigation on 316L/316L-50W/W plate functionally graded materials fabricated by spark plasma sintering, Fusion Eng. Des. 125 (2017) 171–177, https://doi.org/10.1016/j.fusengdes.2017.08.001.

[8] W. Liu, X. Pang, Q. Cai, Y. Ma, W. Zhu, Fabrication of W/steel joint using hot isostatic pressing with Ti/Cu/Ti liquid forming interlayer, Fusion Eng. Des. 135 (2018) 59–64, https://doi.org/10.1016/j.fusengdes.2018.07.013.

[9] Q. Cai, W. Liu, Y. Ma, W. Zhu, X. Pang, Effect of joining temperature on the microstructure and strength of W–steel HIP joints with Ti/Cu composite interlayer, J. Nucl. Mater. 507 (2018) 198–207, https://doi.org/10.1016/j.jnucmat.2018.05.004.

[10] W.W. Basuki, J. Aktaa, Process optimization for diffusion bonding of tungsten with EUROFER97 using a vanadium interlayer, J. Nucl. Mater. 459 (2015) 217–224, https://doi.org/10.1016/j.jnucmat.2015.01.033.

[11] S. Heuer, J. Matějíček, M. Vilémová, M. Koller, K. Illkova, J. Veverka, T. Weber, G. Pintsuk, J.W. Coenen, C. Linsmeier, Atmospheric plasma spraying of functionally graded steel/tungsten layers for the first wall of future fusion reactors, Surf. Coatings Technol. 366 (2019) 170–178, https://doi.org/10.1016/j.surfcoat.2019.03.017.

[12] B.A. Kalin, A.N. Suchkov, V.T. Fedotov, O.N. Sevryukov, A.A. Ivanniko, A. A. Gervash, Brazing of Be with CuCrZr-bronze using copper-based filler metal STEMET, Nucl. Mater. Energy. 9 (2016) 388–393, https://doi.org/10.1016/j.nme.2016.07.004.

[13] A. Gervash, R. Giniyatulin, T. Guryeva, D. Glazunov, V. Kuznetsov, I. Mazul, Ogursky, P. Piskarev, V. Safronov, R. Eaton, R. Raffray, O. Sevryukov, The development of technology of Be/CuCrZr joining using induction brazing, Fusion Eng. Des. 146 (2019) 2292–2296, https://doi.org/10.1016/j.fusengdes.2019.03.175.

[14] B.A. Kalin, A.N. Suchkov, V.T. Fedotov, O.N. Sevryukov, P.V. Morokhov, V. M. Ananiyn, A.A. Ivannikov, A.A. Polyansky, I.V. Mazul, A.N. Makhankov, A. A. Gervash, Brazing of the ITER first wall by a copper-based rapidly quenched ribbon-type filler metal, Fusion Sci. Technol. 65 (2014) 212–221, https://doi.org/10.13182/FST13-667.

[15] A. Elrefaey, High-temperature Brazing in Aerospace Engineering, Woodhead Publishing Limited, 2011, https://doi.org/10.1016/B978-1-84569-532-3.50011-3.

[16] I.S. Logvenchev, A.A. Ivannikov, A.A. Volkov, N.V. Arofikin, O.N. Sevryukov, V. T. Fedotov, A.N. Suchkov, I.V. Fedotov, V.I. Skrytnyi, The brazing of nickel alloys for nuclear reactor with the using of the rapidly-quenched filler metals, Inorg. Mater. Appl. Res. 5 (2014) 263–267, https://doi.org/10.1134/S2075113314030101.

[17] V. Casalegno, F. Valenza, C. Balagna, R. Sedlák, V. Girman, M. Salvo, S. De la Pierre des Ambrois, M. Ferraris, Characterisation of joined surface modified SiCf/SiC composites, Ceram. Int. 46 (2019) 4159–4166, https://doi.org/10.1016/j.ceramint.2019.10.133.

[18] A. Rabinkin, H. Metals, Amorphous brazing foil at age of maturity, Proc. 3 Int. Brazing Solder. Conf. (2006) 10–15.

[19] B. Van der Schaaf, F. Tavassoli, C. Fazio, E. Rigal, E. Diegele, R. Lindau, G. LeMarois, The development of EUROFER reduced activation steel, Fusion Eng. Des. 69 (2003) 197–203, https://doi.org/10.1016/S0920-3796(03)00337-5.

[20] V.M. Chernov, M.V. Leont'eva-Smirnova, E.M. Mozhanov, N.S. Nikolaeva, A. N. Tyumentsev, N.A. Polekhina, I.Y. Litovchenko, E.G. Astafurova, Thermal stability of the microstructure of 12% chromium ferritic–martensitic steels after long-term aging at high temperatures, Tech. Phys. 61 (2016) 209–214, https://doi.org/10.1134/S1063784216020092.

[21] D. Bachurina, A. Suchkov, A. Filimonov, I. Fedotov, M. Savelyev, O. Sevryukov, B. Kalin, High-temperature brazing of tungsten with steel by Cu-based ribbon brazing alloys for DEMO, Fusion Eng. Des. (2019) 0–1, https://doi.org/10.1016/j.fusengdes.2019.02.072.

[22] M.V. Leontyeva-Smirnova, A.N. Agafonov, G.N. Ermolaev, A.G. Ioltukhovsky, E. M. Mozhanov, L.I. Reviznikov, V.V. Tsvelev, V.M. Chernov, T.M. Bulanova, V. N. Golovanov, Z.O. Ostrovsky, V.K. Shamardin, A.I. Blokhin, M.B. Ivanov, E. V. Kozlov, Yu.R. Kolobov, B.K. Kardashev, Microstructure and mechanical properties of low-activated ferritic-martensitic steel EK-181 (RUSFER-EK-181), Prospect. Mater. 6 (2006) 40–52 (In Russian).

[23] P. Norajitra, S. Antusch, R. Giniyatulin, V. Kuznetsov, I. Mazul, H.J. Ritzhaupt-Kleissl, L. Spatafora, Progress of He-cooled divertor development for DEMO, Fusion Eng. Des. 86 (2011) 1656–1659, https://doi.org/10.1016/j.fusengdes.2010.12.005.

[24] R.D. Svetogorov, High-resolution powder diffraction at the XSA beamline of the Kurchatov synchrotron radiation source, Conf. Proc. IX Natl. Cryst. Chem. Conf. (2018) 81.

[25] R.D. Svetogorov, S.N. Sulyanov, Dionis – Diffraction Open Integration Software, 2018660965, n.d.

[26] W.W. Basuki, J. Aktaa, Diffusion bonding between W and EUROFER97 using v interlayer, J. Nucl. Mater. 429 (2012) 335–340, https://doi.org/10.1016/j.jnucmat.2012.05.049.

[27] S.W. Andy Watson Evgenia Lysova, L. Rokhlin, M. Materials Science International Team, Phase diagram of the Cu-V system: Datasheet from MSI Eureka in SpringerMaterials (https://materials.springer.com/msi/phase-diagram/docs/sm_msi_r_20_016228_01_full_LnkDia0), (n.d.). https://materials.springer.com/msi/phase-diagram/docs/sm_msi_r_20_016228_01_full_LnkDia0.

[28] P. Villars, H. Okamoto, eds., Cu-Ti Binary Phase Diagram 0-100 at.% Ti: Datasheet from "PAULING FILE Multinaries Edition – 2012" in SpringerMaterials (https://materials.springer.com/isp/phase-diagram/docs/c_0906918), (n.d.). https://materials.springer.com/isp/phase-diagram/docs/c_0906918.

[29] A.N. Tyumentsev, V.M. Chernov, E.G. Astafurova, N.A. Shevyako, I. Yu. Litovchenko, Features of the microstructure of ferrite-martensitic (12% Cr) steel EK-181 after heat treatment in different modes, J. Tech. Phys. 8/1 (2012) 53–58 (In Russian).

[30] M.A. Penyaz, A.A. Ivannikov, B.A. Kalin, P.S. Dzhumaev, Thermal fatigue damage of steel joints brazed with various nickel filler metals, Non-Ferrous Met. 46 (2019) 33–39, https://doi.org/10.17580/nfm.2019.01.06.

[31] H.Y. Chen, L.M. Luo, J. Zhang, X. Zan, X.Y. Zhu, G.N. Luo, Y.C. Wu, Investigation on W/Fe diffusion bonding using Ti foil and Ti powder interlayer by SPS, J. Nucl. Mater. 467 (2015) 566–571, https://doi.org/10.1016/j.jnucmat.2015.10.045.

[32] J. Wang, J. Huang, H. Sun, X. Gao, W. Wang, Q. Li, C. Xie, X. Wang, Z. Chen, Q. Gao, S. Liu, G. Luo, E ff ect of deuterium on bonding quality of W/Ti/Steel HIP joints in fi rst wall application, Fusion Eng. Des. 138 (2019) 313–320, https://doi.org/10.1016/j.fusengdes.2018.12.010.

[33] J. de Prado, M. Sánchez, A. Ureña, Evaluation of mechanically alloyed Cu-based powders as filler alloy for brazing tungsten to a reduced activation ferritic-martensitic steel, J. Nucl. Mater. 490 (2017) 188–196, https://doi.org/10.1016/j.jnucmat.2017.04.033.

[34] B.A. Kalin, A.N. Suchkov, V.T. Fedotov, O.N. Sevryukov, P.V. Morokhov, V. M. Ananiyn, A.A. Ivannikov, A.A. Polyansky, I.V. Mazul, A.N. Makhankov, A. A. Gervash, Brazing of the ITER first wall by a copper-based rapidly quenched ribbon-type filler metal, Fusion Sci. Technol. 65 (2014) 212–221, https://doi.org/10.13182/FST13-667.